

PHYS134L Final Project

December 6, 2022

1 Introduction

Cooperating with X, I finished two projects this quarter: period estimation of HIP320 and stellar effective temperature estimation algorithm.

2 Period Measurement of a Short-Period RR Lyrae Star

Variable stars are stars that change brightness, and they are an important part of our university. For now, there are over 1,000,000 stars known and cataloged, and many thousands more are suspected to be variable [3]. Research on variable stars is important because it provides information about stellar properties, such as mass, radius, luminosity, temperature, internal and external structure, composition, and evolution [7]. Variable stars need to be systematically observed over decades in order to determine their long-time behavior. In this work, I present our method and process of measuring a short-period RR Lyrae star.

The RR Lyrae(RR Lyr) stars are identified with a unique stage in the life of a low-mass star, the horizontal branch, helium core burning period of evolution. As such, they show a small range in luminosity, the most variable property being their effective temperature as a function of mass [2].

In this section, I present our measurement of HIP320, a short-period RR Lyrae star, and the method of estimating its variation pattern.

2.1 Introduction

The study of RR Lyrae Variables is important for our understanding of the universe. First, The RR Lyr stars are best studied as members of globular clusters, where they appear in large



Figure 1: HIP320 is in the middle of this figure.

numbers because of the sizable population of the horizontal branch in these evolved stellar systems. They can be classified according to a metallicity index, first proposed by Preston, which compares the spectral type assigned from the metal lines, especially Ca II, to that obtained from the hydrogen Balmer lines [4].

Second, the RR Lyrae Variables serve as important standard candles that are used to measure astronomical distances [5]. A standard candle is a class of astrophysical objects, such as supernovae or variable stars, which have known luminosity due to some characteristic quality possessed by the entire class of objects. Thus, if an extremely distant object can be identified as a standard candle, then the absolute magnitude M of that object is known. Thus, the distance D can be calculated from the apparent magnitude m as shown below

$$M = m - 97.5 + 5 \log(D) \quad (2.1)$$

RR Lyrae Variables are usually closer to the center of the galaxy and halo, which can provide the measurement of the distance of the area near the galactic center.

Accurate photometry data are the first prerequisite for such studies because we need such quantities as mean light intensity, interstellar reddening, blanketing, and especially in connection with the last and first points, temperature, surface gravity, and radius variation.

Table 1: LCO’s Filter Parameters

| Filter Name | WavelengthCenter(Å) | Wavelength Width(Å) |
|-------------|---------------------|---------------------|
| Bessell B | 4361 | 890 |
| Bessell V | 5448 | 840 |

Table 2: Photometry Information of Calibration Stars

| Star ID | Catalog | m_B | m_V |
|----------------|----------------------|--------|--------|
| TYC 5838-825-1 | 2014 Hypatia Catalog | 13.022 | 12.341 |
| BD-17 6869 | 2000 Tycho-2 Catalo | 11.07 | 10.00 |
| BD-17 6867 | 2000 Tycho-2 Catalo | 11.05 | 10.50 |

2.2 Method

2.2.1 Photometry

Our observation took place on 23rd November at the Las Cumbres Observatory(LCO) in Santa Barbara. By using LCO’s 0.4-meter telescope, nine measurements were taken in Bessell B and Bessell V bands. The details of the filter information are shown in table 1.

In order to obtain the apparent magnitude in each band, three calibration stars are utilized: BD-17 6869, BD-17 6867, and TYC 5838-825-1. As shown in Figures 2 and 3, the target star HIP320 is marked with a yellow circle, while the three calibration stars are marked with red circles. By calling the python package `photutils.aperture`, the flux F_x can be obtained. Then, the magnitude without calibration is given by

$$m_x = -2.5 \times \log_{10}(F_x) \tag{2.2}$$

where x stands for the specific spectral band. The calibration magnitude of TYC 5838-825-1 is obtained from the Hypatia Catalog [1], while the calibration magnitudes of BD-17 6869 and BD-17 6867 are obtained from the Tycho-2 Catalog [2]. The photometry information of the calibration stars is listed in table 2.

The calibration magnitude and the zero point are calculated by the following formula

$$\text{zero_point} = \sum (m_{raw} - m_{cal}) \times \frac{1}{3} \tag{2.3}$$

where m_{raw} is the uncalibrated magnitude obtained directly by the flux in our measurement. Then, the apparent magnitudes of each are matched with the observation time, which is listed in table 3 and table 4.

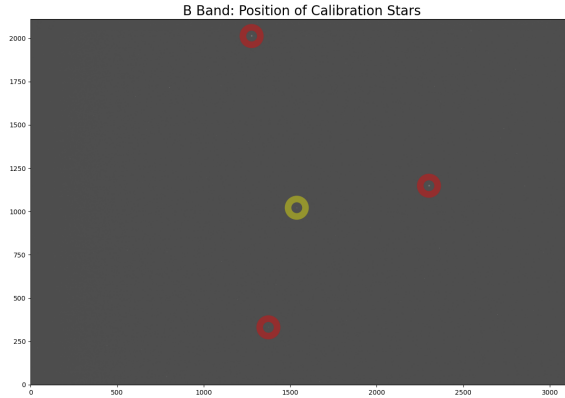


Figure 2: Calibration stars in B band

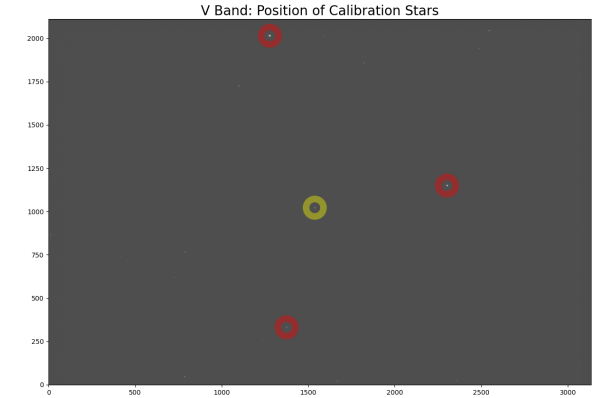


Figure 3: Calibration stars in V band

Table 3: Time v.s. The magnitude of HIP320 in B band

| | | | | | | | | |
|--------|--------|--------|--------|--------|--------|--------|--------|--------|
| 00:25 | 00:56 | 03:25 | 04:58 | 07:20 | 9.59 | 10:59 | 19:31 | 21:15 |
| 12.491 | 12.276 | 12.227 | 12.331 | 12.574 | 12.850 | 12.780 | 12.382 | 12.571 |

2.2.2 Period Estimation

Because of a lack of data, the specific pattern of variation of HIP320 cannot be assumed from our data. Therefore, I assume that its brightness varies in a sine-like function. Based on this assumption, python's `scipy.optimize` package is utilized to fit the given data and estimate the most-likely period.

The `scipy.optimize` provides a 'curve_fit' function in its optimization library to fit the data with a given function. This method applies non-linear least squares to fit the data and extract the optimal parameters out of it. The initial guess plays a significant role in this fitting. The function fits the given data based on the initial guess and minimizes the least square. The initial amplitude A is given by

$$A = \sqrt{2}\sigma_{mag} \quad (2.4)$$

where the σ_{mag} is the standard deviation of magnitude in each band. The initial offset is the average magnitude. Then, based on Hipparcos's variable star catalog, the period of HIP320 is 14.5 hours, which is considered as the initial frequency guess. [3].

The fitting results of each band are shown in table 5.

Table 4: Time v.s. The magnitude of HIP320 in the V band.

| | | | | | | | | |
|--------|--------|--------|--------|--------|--------|--------|--------|--------|
| 00:25 | 00:58 | 03:27 | 04:58 | 07:21 | 10:02 | 11:01 | 19:34 | 21:18 |
| 11.949 | 11.758 | 11.719 | 11.776 | 11.946 | 12.280 | 12.109 | 11.804 | 12.011 |

Table 5: Fitting results

| Band | Amplitude | Angular freq | Phase | Offset |
|--------|-----------|--------------|----------|----------|
| V band | 0.24852 | 0.45334 | 3.167026 | 11.94207 |
| B band | 0.29796 | 0.44701 | 3.29360 | 12.51928 |

2.3 Results

After the analysis is done by python, the plots with the fitting result are obtained. By B band data, the amplitude of variation is 0.298mag, so the maximum variation is about 0.596mag. The average magnitude is 13,65mag. Then the period can be calculated out from frequency as 14.05 hours. By V band data, the amplitude of variation is 0.249mag, so the maximum variation is about 0.599mag. The average magnitude is 11.94mag. Then the period can be calculated out from frequency as 14.05 hours. The error bars shown in plots are obtained while calculating the zero point by the calibration stars.

According to the data of Hipparcos Variability Annex [4], the period of HIP320 is 0.606 days, about 14.4 hours. So the percent error is approximately 2.43%, which is relatively small that we can conclude our result is accurate.

Caused by the quality of data and time of observation, there are many limitations in our work. Based on our results, the error bar in the B band is relatively smaller than in the V band. Although the period is closely accurate, it might still be influenced by a couple of factors. Although the calibration stars used are the same in both bands, there is a small fluctuation of BD-17 6867's brightness in the V band, which causes the standard error of zero point to be larger in the V band data. Moreover, we assume that the variation pattern of HIP320 is a sine-like function. However, most of the variable stars do not behave like a sine function. Therefore, the model based on the sine function may not be the best option here.

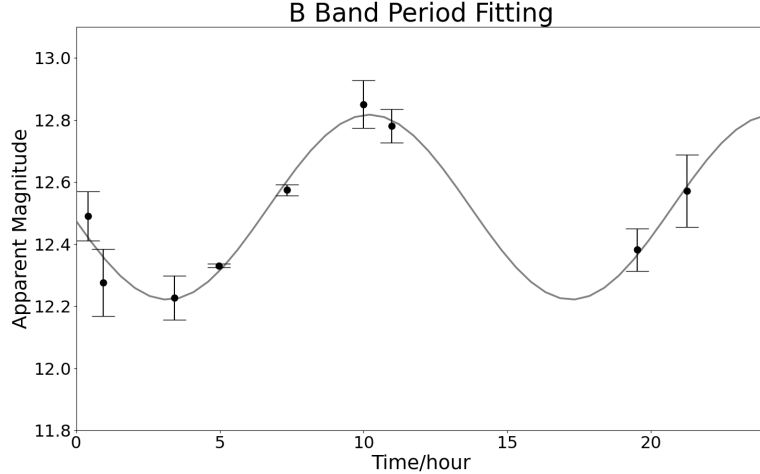


Figure 4: The diagram shows the relation between the magnitude and time of the V band. The average magnitude is 11.94, slightly smaller than in the B band.

2.4 Discussion

We observed a short-period RR Lyrae variable star, HIP320 by the LCO, and estimated its possible variation pattern. Based on our fitting result, the best-estimated period is 13.65 hours in the V band and 14.05 hours in the B band, which are close to the data of the Hipparcos Variability Annex.

The photometry of RR Lyrae star, like HIP320, is significant for the study of stellar population and estimation of distance as standard candles. Since they serve as tracers and distance indicators of old stellar populations in the Milky Way and neighboring galaxies, they are also essential laboratories for testing evolutionary and pulsation models. Nowadays, more and more sky-survey programs, including Sloan Digital Sky Survey(SDSS) and COSMOS survey, started to focus on the study and measurement of variable stars. The latest edition of the General Catalogue of Variable Stars lists more than 46,000 variable stars in the Milky Way, as well as 10,000 in other galaxies and over 10,000 'suspected' variables [6].

3 Temperature Estimation based Blackbody Model

The effective temperature is one of the fundamental parameters that characterize a star. Theoretically, the effective temperature of a star is the temperature of a black body of the same size as the star, and that would radiate the same total amount of electromagnetic power

as emitted by the star, which is given by the Stefan–Boltzmann law

$$T_{eff} = \sqrt[4]{\frac{P}{4\pi R^2\sigma}} \quad (3.1)$$

where P is the power radiated by a star of radius R and σ is the Stefan–Boltzmann constant that equals to $5.67037 \times 10^{-8} W m^{-2} K^{-4}$ [14].

Effective temperature serves as one of the most fundamental stellar parameters. It is directly related to the color of the star: the higher the temperature, the bluer the light emitted by the star. The effective temperature is one of the two parameters, with the stellar luminosity, used to build the classical HR diagram that permits astronomers to classify stars.

In this section, I present my method of estimation of effective temperature using the high-resolution spectrums from the SDSS-IV MaStar library.

3.1 Introduction

While estimating stellar effective temperature, astronomers mainly use three techniques: Wien’s Displacement Law, color–temperature relationship, and spectrum analysis of a star. Wien’s law is concerned with the radiation spectrum of a black body. According to it, the blackbody radiation curve for different temperatures will peak at different wavelengths that are inversely proportional to the temperature [14]. Therefore, the peak of power radiation occurs at the wavelength given by

$$\lambda_{peak} = \frac{2.898 \times 10^{-3} mK}{T_{eff}} \quad (3.2)$$

However, this is only applicable to stars with spectra that closely approximate that of a blackbody [13]. Moreover, the flux-calibrated spectra of the star under consideration should also be available.

Another method to measure the temperature of stars is by analyzing their color index. The color index of a star is defined as the difference between two measurements of the magnitude (brightness on a logarithmic scale) of a star made at different wavelengths, the value found at the longer wavelength being subtracted from that found at the shorter. The measurements from the photometer are converted to temperature using standard scales. A good approximation can be obtained by considering stars as black bodies, using Ballesteros’ formula, which is given by

$$T_{eff} = 4600K \left(\frac{1}{0.92(B - V) + 1.7} + \frac{1}{0.92(B - V) + 0.62} \right) \quad (3.3)$$

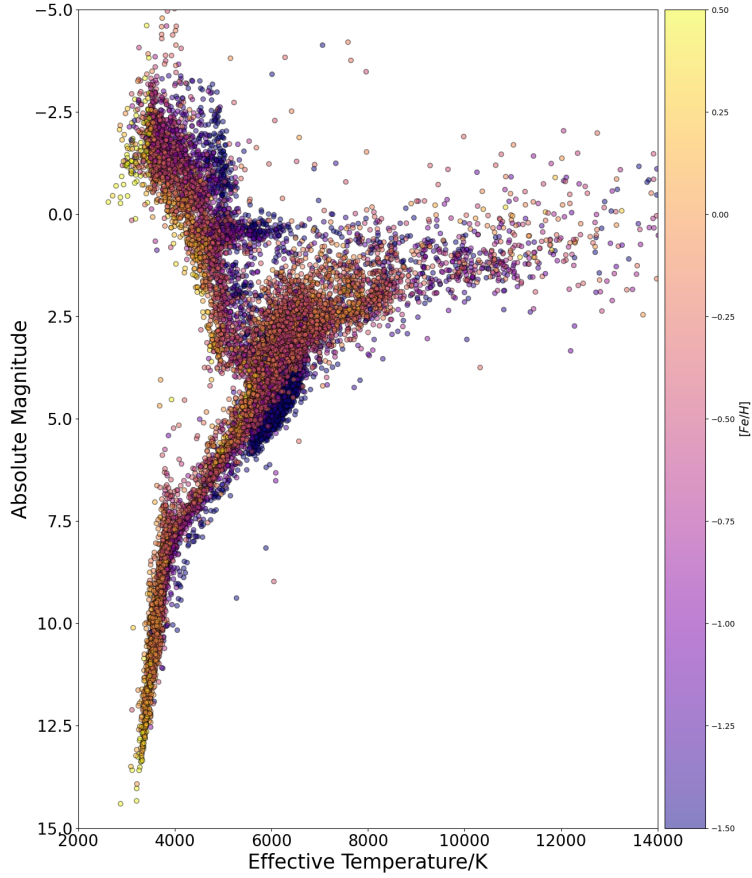


Figure 5: HR Diagram of MaStar Library

where B and V stand for the magnitude in the B band and V band. This method is beneficial when a good spectrum of a star is not available. The results obtained in this method are accurate up to $\pm(100 - 200)K$. However, this method gives poor results for cooler stars.

In this work, I estimate the effective temperature from the analysis of spectra. I fit the spectra with the blackbody model. The blackbody is a theoretical or model body that absorbs all radiation falling on it, reflecting or transmitting none. Usually, the Planck law of blackbody radiation is used to determine the spectral energy density of the emission at each wavelength E_λ at a particular absolute temperature T , which is given by

$$E_\lambda = \frac{8\pi hc}{\lambda^5(e^{hc/\lambda kT} - 1)} \quad (3.4)$$

where k is the Boltzmann constant, h is the Planck constant, and c is the speed of light.

3.2 Method

3.2.1 Data Model

In this work, I used the published spectra data library by SDSS’s MaStar. The SDSS-IV MaStar is a large, well-calibrated, high-quality empirical library aiming at observing more than 10,000 individual stars whose spectra cover the wavelength range of $3,622 - 10,354\text{\AA}$ at a resolution of 1800 [12]. This library is easily accessible by python and is suitable for batch and bulk data processing. In this work, we utilize the DR17 version of the MaStar Library.

Four catalogs are downloaded from SDSS. ‘mstar_goodstars_xmatch_gaiaedr3’ contains detailed photometry information, and it provides crossmatch between MaStar and Gaia EDR3, 2MASS, Simbad, and PanSTARRS1. The ‘mstarall-dr17.fits’ file is a summary table containing information on the MaStar target, including the MaNGA ID, locations, PSF Magnitude, input parameters, radial velocity, spectral quality flags, and more. All high-quality 1D MaStar spectra are located in the ‘mstar-good spec-dr17.fits’ file. The stellar parameters of a subset of selected stars, including effective temperature, surface gravity, and chemical composition, are contained in ‘mstar-goodstar-dr17.fits’ [8].

In this work, by using stellar parameters provided by MaStar’s model, 11 A type and B type stars are selected. Typically, B type stars are blue-white stars with temperatures $10000 - 30000K$, while A type stars are blue stars with temperatures $7000 - 10000K$. B stars are hot stars defined by the presence of hydrogen (H) and neutral helium (HeI) in the optical spectra. H line strength increases over the B star subclasses while HeI decreases. The A type stars have the Strongest H lines.

3.2.2 Heliocentric Velocity Correction

Due to the motions of the Earth around the Sun, the observed wavelength of the stars is affected by the Doppler effect induced by the spacecraft velocity component in the direction of the target [9]. Therefore, the first step is to correct the spectra to rest-frame. The corrected wavelengths are defined as

$$\lambda_{rest} = \left(1 + \frac{v}{c}\right)\lambda_{raw} \quad (3.5)$$

where v is defined as the Heliocentric velocity that are provided in MaStar’s spectrum catalog.

MaNGA ID:3-139907354

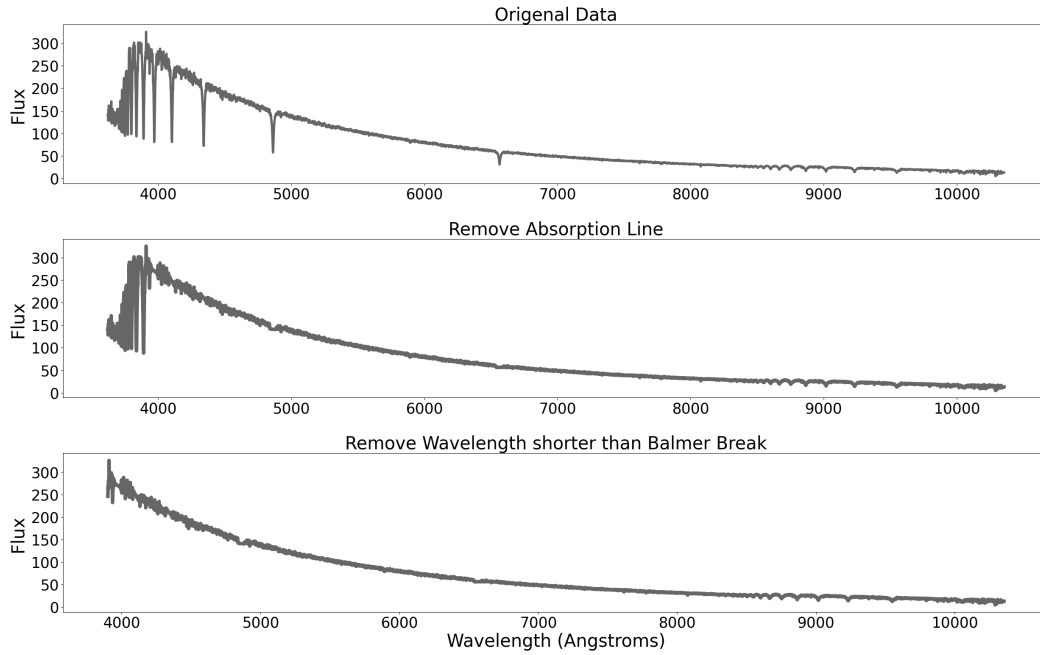


Figure 6: Removing absorption lines

3.2.3 Absorption Line

The absorption line can be used to determine the chemical abundance in stellar atmospheres, but it will also influence the fitting process. Therefore, the second step is to eliminate the absorption line from the data, and only the range of wavelength without obvious absorption can be used for temperature fitting.

Since the spectra cover the wavelength range starting from 3622\AA , the Balmer break can exert a significant influence on temperature fitting. Balmer break is defined as the difference of intensity of the stellar continuum spectrum on either side of the limit of the Balmer series of hydrogen, at 3646\AA in the rest frame. Hydrogen (H) lines, including the closely spaced absorption features that disappear at the Balmer break, are strongest in Type A stars. Therefore, my first step is to determine whether there is a Balmer break in the given spectra. If so, I removed the data with wavelength $\lambda < 3900\text{\AA}$.

For other absorption lines, I build a list that contains the most common absorption line wavelengths. Then, I remove the absorption line if there is a sudden drop near the assigned wavelength. In figure 6, it shows the process that data are processed step by step.

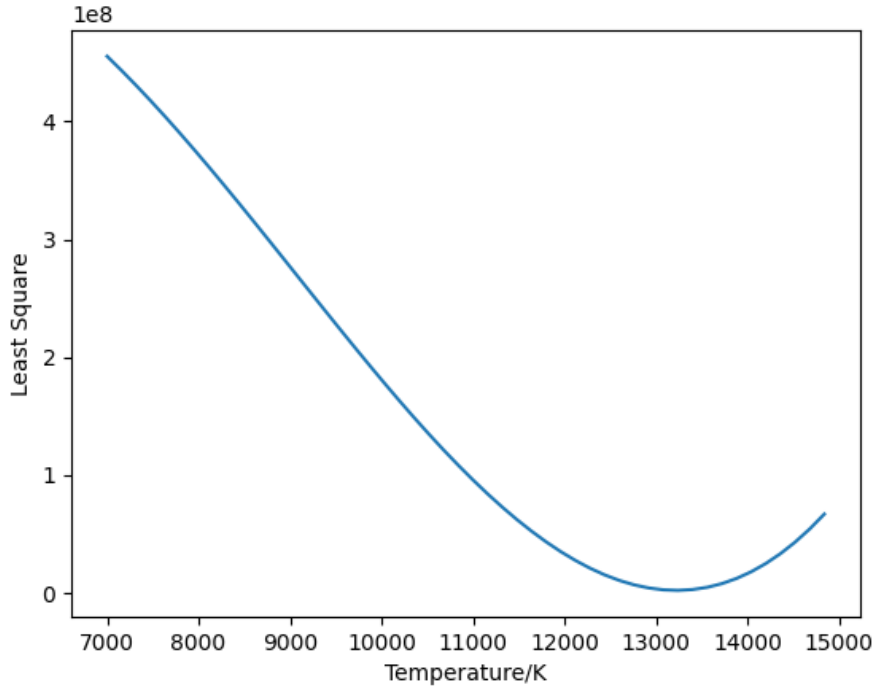


Figure 7: Least Square Method

3.2.4 Least Square Fitting

The least-square fitting method is a mathematical procedure for finding the best-fitting curve to a given set of points by minimizing the sum of the squares of the offsets of the points from the curve. The equation is given by

$$R^2 = \sum (y_i - f(x_i))^2 \quad (3.6)$$

The sum of the squares of the offsets is used instead of the offset absolute values because this allows the residuals to be treated as a continuously differentiable quantity. By comparing the flux in spectra and the black body radiation model, the best-estimated temperature can be obtained by finding the lowest least-square. The figure 7 shows one of the fitting process.

The least-square method is taken five times for each spectrum, and after each process, the data point that is much lower than the fitting line will be eliminated. This step is used to reduce some indistinct absorption lines that are not included in the previous list.

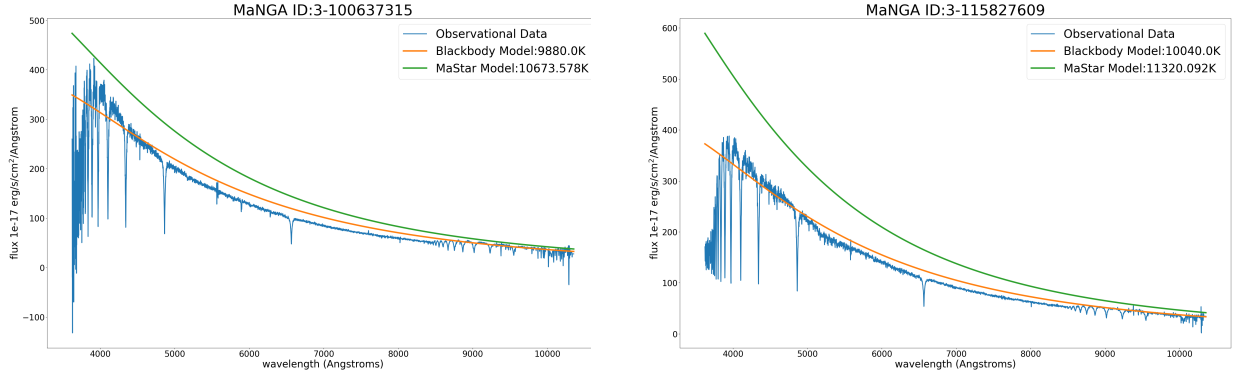


Figure 8: Temperature Fitting of Stars with Obvious Balmer Break

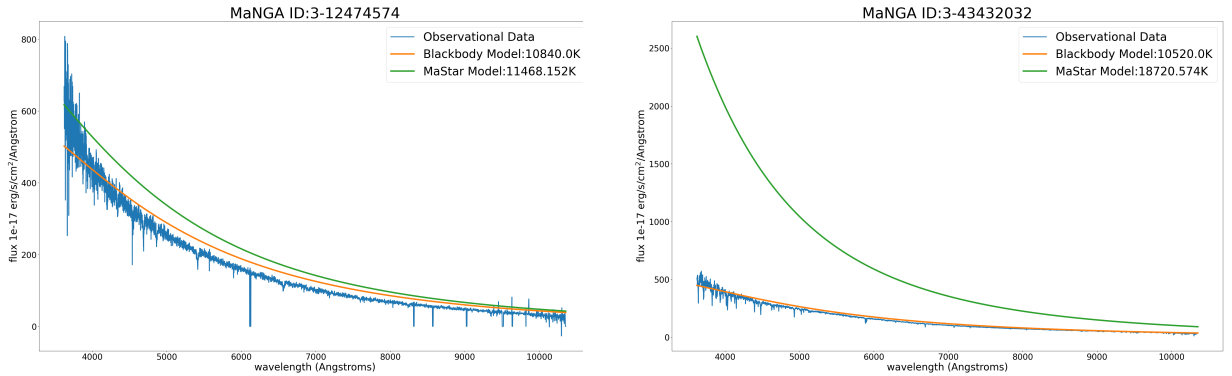


Figure 9: Temperature Fitting of Stars without Obvious Balmer Break

3.3 Results

The temperature estimation has done for 11 A type and B type stars in MaStar’s library.

In figure 8 and figure 9, it shows some fitting results. The orange lines my fitting results, while the green lines are based on T_{eff} of the MaStar’s model. For most of the cases, my fitting results are relatively lower than that of the MaStar’s model.

This paper presents a very simple method for temperature estimation by spectra fitting. Figure 10 compares the results from my method and that of the MaStar’s model. Based on this plot, it is clear that temperatures from MaStar’s model are usually higher than my results. In MaStar library, they fit theoretical spectra from model atmospheres by both MARCS and BOSZ-ATLAS9 to the observed MaStar spectra, using the full spectral fitting code pPXF. For short, both of these models are combined theoretical stellar atmospheres models and empirical observations [11]. Therefore, MaStar’ model should be much more accurate and precise.

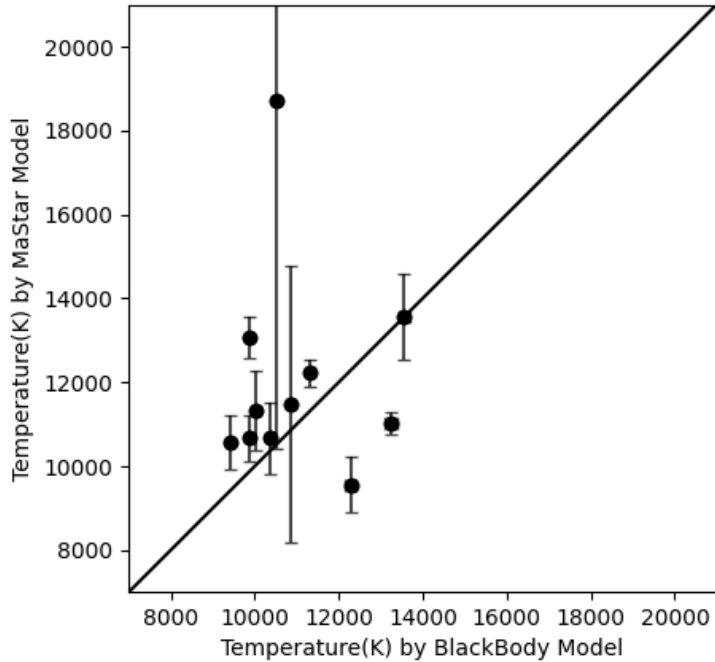


Figure 10: Comparing Two Models

This paper presents a very simple method for temperature estimation by spectra fitting. Figure 10 compares the results from my method and that of the MaStar’s model. Based on this plot, it is clear that temperatures from MaStar’s model are usually higher than my results. In MaStar library, they fit theoretical spectra from model atmospheres by both MARCS and BOSZ-ATLAS9 to the observed MaStar spectra, using the full spectral fitting code pPXF. For short, both of these models are combined theoretical stellar atmospheres models and empirical observations [11]. Therefore, MaStar’ model should be much more accurate and precise.

3.4 Discussion

Based on my assumption, one of the reasons that my results are relatively lower is that stars are far from a perfect black body since the gas of the star’s atmosphere absorbs and emits light, creating deep absorption and emission lines in the spectrum we observe. Also, the existence of the interstellar medium(ISM) may also influence heavily on the spectra [10].

Also, for now, this simple algorithm can only deal with high-temperature A-type and B-type stars, which are only a small part of the stellar population. Furthermore, the absorption line should also be considered while fitting to obtain a more precise result. Most widely-used

temperature estimation algorithms are combined both theoretical stellar model and observational data with high confidence.

Measurement and estimation of stellar temperature are always fundamental for the study of stellar evolution. Nowadays, with the development of machine learning and our understanding of the stellar atmosphere, more accurate and efficient algorithms are being developed.

References

- [1] Hinkel, N. R., Timmes, F. X., Young, P. A., Pagano, M. D., and Turnbull, M. C., “Stellar Abundances in the Solar Neighborhood: The Hypatia Catalog”, *The Astronomical Journal*, vol. 148, no. 3, 2014. doi:10.1088/0004-6256/148/3/54.
- [2] Høg, E., “The Tycho-2 catalogue of the 2.5 million brightest stars”, *Astronomy and Astrophysics*, vol. 355, pp. L27–L30, 2000.
- [3] Perryman, M. A. C., “The HIPPARCOS Catalogue”, *Astronomy and Astrophysics*, vol. 323, pp. L49–L52, 1997.
- [4] Robert A. Meyers, ”Encyclopedia of Physical Science and Technology”, Third Edition, 2021 978-0-12-227410-7
- [5] Bhardwaj, Anupam. “Cepheid and RR Lyrae Variables as Standard Candles and What Else.” *arXiv: Solar and Stellar Astrophysics* (2018): n. pag.
- [6] Samus, N. N., Durlevich, O. V., and et al., “VizieR Online Data Catalog: Combined General Catalogue of Variable Stars (Samus+ 2004)”, *VizieR Online Data Catalog*, 2004.
- [7] Braga, V. F., “On the use of field RR Lyrae as galactic probes - VI. Mixed mode RR Lyrae variables in Fornax and in nearby dwarf galaxies”, *Monthly Notices of the Royal Astronomical Society*, vol. 517, no. 4, pp. 5368–5381, 2022. doi:10.1093/mnras/stac2813.
- [8] Lazarz, D., “SDSS-IV MaStar: Stellar parameter determination with continuum-supplemented full-spectrum fitting”, *Astronomy and Astrophysics*, vol. 668, 2022. doi:10.1051/0004-6361/202243701.
- [9] Cho, K., Testa, P., De Pontieu, B., and Polito, V., “A Statistical Study of the IRIS Observational Signatures of Nanoflares and Non-thermal Particles”, *arXiv e-prints*, 2022.

- [10] Imig, J., “SDSS-IV MaStar: Data-driven Parameter Derivation for the MaStar Stellar Library”, *The Astronomical Journal*, vol. 163, no. 2, 2022. doi:10.3847/1538-3881/ac3ca7.
- [11] Hill, L., “SDSS-IV MaStar: theoretical atmospheric parameters for the MaNGA stellar library”, *Monthly Notices of the Royal Astronomical Society*, vol. 509, no. 3, pp. 4308–4329, 2022. doi:10.1093/mnras/stab3263.
- [12] Yan, R., “SDSS-IV MaStar: A Large and Comprehensive Empirical Stellar Spectral Library—First Release”, *The Astrophysical Journal*, vol. 883, no. 2, 2019. doi:10.3847/1538-4357/ab3ebc.
- [13] Debnath, S., “A note on stellar ionization”, *New Astronomy*, vol. 98, 2023. doi:10.1016/j.newast.2022.101926.
- [14] Yuan, H.-B., “The miniJPAS survey: stellar atmospheric parameters from 56 optical filters”, *Monthly Notices of the Royal Astronomical Society*, vol. 518, no. 2, pp. 2018–2033, 2023. doi:10.1093/mnras/stac3155.